

Efficient methodology for multibody simulations with discontinuous changes in system definition

Rudranarayan M. Mukherjee · Kurt S. Anderson

Received: 27 February 2007 / Accepted: 4 June 2007 / Published online: 18 July 2007
© Springer Science+Business Media B.V. 2007

Abstract A new method is presented for accurately and efficiently simulating multi-scale multibody systems with discontinuous changes in system definitions as encountered in adaptive switching between models with different resolutions as well as models with different system topologies. An example of model resolution change is a transition of a system from a discrete particle model to a reduced order articulated multi-rigid body model. The discontinuous changes in system definition may be viewed as an instantaneous change (release or impulsive application of) the system constraints. The method uses a spatial impulse–momentum formulation in a divide and conquer scheme. The approach utilizes a hierarchic assembly–disassembly process by traversing the system topology in a binary tree map to solve for the jumps in the system generalized speeds and the constraint impulsive loads in linear and logarithmic cost in serial and parallel implementations, respectively. The method is applicable for systems in serial chain as well as kinematical loop topologies. The coupling between the unilateral and bilateral constraints is handled efficiently through the use of kinematic joint definitions. The equations of motion for the system are produced in a hierarchic sub-structured form. This has the advantage that changes in sub-structure definitions/models results in a change to the system equations only within the associated sub-structure. This allows for significant changes in model types and definitions without having to reformulate the equations for the whole system.

Keywords Impulse momentum formulation · Divide and conquer scheme · Logarithmic complexity · Course-graining of models · Discontinuous system definitions

R.M. Mukherjee is now at Jet Propulsion Laboratory, Pasadena, California

R.M. Mukherjee (✉) · K.S. Anderson

Department of Mechanical, Aeronautical, and Nuclear Engineering, Rensselaer Polytechnic Institute,
Troy, NY 12180, USA

e-mail: rudranarayan.m.mukherjee@jpl.nasa.gov

K.S. Anderson

e-mail: anderk5@rpi.edu

1 Introduction

Multibody dynamics methods are being used in multi-scale modeling in computational studies of important physical phenomena occurring at different spatial and temporal scales. These applications involve the modeling of polymer melts, polymers in aqueous solutions, proteins, DNA, and biomolecules among others. These systems are characterized by large model size spanning thousands (10^3 – 10^4) of degrees of freedom and the simulations involve temporal domains ranging from femto to micro (10^{-15} – 10^{-3}) seconds. Given the large spatial and temporal complexity involved in modeling these systems, intelligent modeling schemes are employed in an effort to alleviate the computational expense. Adaptive imposition of constraints for the purpose of achieving model reduction is one such scheme. In this approach, the large-scale full fidelity fine resolution model of a system is transformed into a comparatively coarser scale and less expensive system by adaptive imposition of constraints. These constraints reduce the model to a more economical one that retains the essential dynamics using a well chosen lower fidelity model. For example, in a biomolecular system, the overall conformational motion may be well captured using an articulated multi-body model while the full fidelity model has to be studied using fully atomistic fine scale resolution. However given the wide variety of properties that these simulations aim at capturing, it often becomes necessary to switch between different resolutions during the course of a simulation. Examples of this switching are the transitions from a fully atomistic model to an articulate multi-rigid body model, and then to an articulated flexible body model without adversely effecting the ability to represent the overall conformational behavior. This is often done to allow larger temporal integration time steps. These adaptive impositions of constraints give rise to discontinuous changes in the system definition during the course of a simulation.

Transition between different levels of model refinement during a simulation is achieved by effectively constraining, adding, or changing the nature of certain degrees of freedom as one moves from a fine scale model to a reduced order model (or vice versa). These changes take place instantaneously during the course of a simulation and as such may be viewed as system model changes resulting from impulsively applied constraints. These transitions result in discontinuous change in the number and/or nature of system degrees of freedom. Another important aspect is the efficient and accurate handling of systems with topological changes. Examples of topology changes include the forming or breaking of bonds, where the bonds are treated as kinematic joints as opposed to stiff springs. Topology changes are also found in phenomena like docking or the formation of hydrogen bonds as found in modeling proteins where the system changes from a serial chain to a system with kinematically closed loops.

Both of these systems, i.e., systems where certain degrees of freedom are instantaneously constrained (or unconstrained) and systems where loops are formed (or broken), are typically classified as systems with unilateral constraints and/or bilateral constraints. This class of problems includes systems where certain constraints are switched from active to inactive or vice versa based on certain criteria. These constraints are not continuous in time and result in the system definition switching discontinuously during the course of a simulation. During the switching of an unilateral constraint, the structure of the equations and the constraints change in a discontinuous fashion, potentially requiring the reformulation of the equations of motion and disruption of the temporal integration scheme. This can result in significant computational expense unless efficient schemes are employed. Moreover, unless a consistent and correct set of generalized speeds are calculated for further simulation of the system after the discontinuous change, the results obtained produce physically incorrect dynamics behavior of the system.

Two broad classes of approaches may be employed to model these systems. The first class of approaches is based on contact mechanics where local deformation models are used. This approach [1, 2] is recommended when the focus of the study is to understand the events in the immediate vicinity of the discontinuous event, i.e., when a detailed understanding of the effect of the discontinuous event is desired. Such an approach can provide excellent insight into the event, but limits the simulation to sufficiently small spatial and temporal domains. Additionally, such formulations are inclined to produce stiff systems of equations that are computationally expensive. This computationally expensive approach is not useful when the focus is to study the overall dynamics of the system over long temporal domains. The second approach [3–13] is thus often employed in these studies where the discontinuous event is instead modeled using a momentum formulation through kinematic constraints and impulsive loads and is suitable for large temporal simulations. In this approach, the complementarity formulation is often used resulting in a set of Differential Algebraic Equations (DAE) with appropriate constraints. These methods have found application and success in modeling systems with many bodies and many unilateral constraints, for example in the simulation of granular materials with potentially many contacts/impacts [4, 14]. The DAE formulations typically result in a sparse, large set of equations that can be solved using specialized sparse solvers. However there exist some numerical issues in the treatment of the impulse momentum formulations using a differential algebraic set of equations [11, 15].

State space formulations [16–19] have been used in multibody dynamics to alleviate the traditional numerical difficulties of DAE formulations [15]. The state space formulations extract a set of Ordinary Differential Equations (ODEs) from the DAE formulation by explicitly embedding the constraints in the governing equations. State space formulations have been used in the past [20, 21] for solving the class of momentum–impulse problems discussed above. Traditionally, these formulations result in a set of n coupled equations, where n is the number of degrees of freedom in the system. The computational cost associated with forming these equations and their subsequent decomposition for solution is typically expensive, requiring $O(n^3)$ computations. This can be a significant computational expense particularly when the number of degrees of freedom are large as is encountered in biomolecular systems and other microscopic systems. Moreover, these approaches are not well adapted for treatment of kinematically closed loops as encountered in systems with bilateral constraints. Further when studying complementarity type problems, these result in undesirable coupling between the bilateral and unilateral constraints.

A new algorithm is presented in this paper for accurately and efficiently simulating multibody systems with discontinuous changes in system definitions with the objective of correctly capturing the nonlinear coupling arising from the articulated nature of the multibody systems. The impulse–momentum formulation is implemented using a sub-structured approach in a divide and conquer scheme [22, 23]. The algorithm utilizes the definition of joint free-motion map (or partial velocities) in calculating the generalized relative velocities between bodies that are connected together by kinematic joints. The method implements a hierarchic assembly–disassembly process by mapping the bodies in the system to a binary tree. This process couples together the impulse–momentum equations of the individual bodies to formulate and solve the corresponding equations for the whole system. This results in an inherently sub-structured form of equations within the formulation making it highly conducive to adjusting/modifying model types within a sub-structure. This is because such a change only affects the sub-structure equations and does not require a change in the global equations. The algorithm is applicable to general systems with either tree or loop topologies. The constraint violations are minimum and the procedure is applicable even when a system is in what would traditionally be considered a singular configuration. Further, this method

is able to maintain linear and logarithmic complexity in serial and parallel implementations, respectively. The reader should, however, note that though this method is extremely successful in the class of problems studied here, it may not be best suited for simulating the generic class of contact–impact problems, especially when encountering systems with potentially many impacts and rebounds.

In the next section, the analytical preliminaries required for the development of the algorithm are presented. The derivation for the recursive formulae is presented next. The hierarchic assembly–disassembly process is then discussed which includes the discussion on the methodology for dealing with loops and chains. Results of numerical test cases to validate the algorithm are then presented followed by a brief discussion on the results.

2 Analytical preliminaries

An articulated multibody system consists of individual rigid and/or flexible bodies connected together by kinematic joints. Depending on the topology, the system can be classified as serial chain, tree or kinematically closed loop(s). These joints allow relative motion between bodies through the joint degrees of freedom. In the absence of a kinematic joint, two bodies can move with respect to each other through 6 degrees of freedom. So the free-motion map between the bodies is a rank 6 matrix. A kinematic joint constrains the relative motion between two bodies. Thus, the kinematic joint partitions the 6 dimensional relative free-motion map between two bodies into the free-motion map P which is of dimension $6 \times \text{dof}$ and its orthogonal complement D of dimension $6 \times (6 - \text{dof})$, where dof is the number of degrees of freedom allowed by the joint. The joint allows free relative motion in the space spanned by the columns of the joint free-motion map P . The joint cannot support a constraint load in the space spanned by P . However the constrained degrees of freedom are mapped by the columns of D and the joint can support constraint loads in the space spanned by this matrix. For example, in case of a representative spherical joint J^k , the translational degrees of motion are constrained while the rotational degrees of freedom are maintained. Hence, the corresponding maps maybe given by

$$P^{J^k} = \begin{bmatrix} 1 & 0 & 0 \\ 0 & 1 & 0 \\ 0 & 0 & 1 \\ 0 & 0 & 0 \\ 0 & 0 & 0 \\ 0 & 0 & 0 \end{bmatrix}, \quad D^{J^k} = \begin{bmatrix} 0 & 0 & 0 \\ 0 & 0 & 0 \\ 0 & 0 & 0 \\ 1 & 0 & 0 \\ 0 & 1 & 0 \\ 0 & 0 & 1 \end{bmatrix}. \tag{1}$$

From a linear algebra point of view, the joint free-motion map P can also be interpreted as the $6 \times \text{dof}$ matrix that maps the dof generalized speeds u associated with the relative free motion permitted by a joint into a 6×1 column matrix of spatial relative velocity which may occur across the joint.

It is apparent from their definitions, the orthogonal complement D^{J^k} and the joint free-motion map P^{J^k} of any representative kinematic joint between two representative bodies k and $k + 1$, satisfy the following orthogonality relation

$$(P^{J^k})^T \cdot D^{J^k} = 0 \quad \text{and} \quad (D^{J^k})^T \cdot P^{J^k} = 0. \tag{2}$$

A term introduced in [22] and used continually in the paper is *handle*. A handle is any selected point on the body which is used in modeling the interactions of the body with the

environment. The handles on a body can correspond to a joint location, a center of mass or any desired reference point. For modeling convenience, the handles can even be selected so as to coincide. A body can have any number of handles on it. While the joint locations are chosen as handles on the body for the analytical discussions presented here, this is not a restrictive choice.

Another term used in this paper is *event*. An event describes any discontinuous change in system definition. This includes specific joints definitions being changed and the formation or breaking of kinematic loops as found in unilateral and bilateral constraints.

The equations derived in the next section are in the format of spatial vectors and tensors as presented in [24]. For example, the spatial velocity vector of the center of mass on body k is shown in (3). Similarly, the spatial inertia tensor of rigid body k about its center of mass is shown in (4).

$$\mathcal{V}_0^k = \begin{bmatrix} \omega_0^k \\ v_0^k \end{bmatrix}, \tag{3}$$

$$\mathcal{M}_0^k = \begin{bmatrix} I_0^k & \underline{0} \\ \underline{0} & m^k \end{bmatrix}. \tag{4}$$

In the above, the subscript 0 denotes the center of mass of the body, while superscript k indicates that the quantity is associated with representative body k . \mathcal{M}_0^k is the 6×6 spatial inertia matrix of body k about the point 0 and is composed of the 3×3 inertia matrix of body k about its mass center, the 3×3 diagonal mass matrix m^k in which each diagonal element of the matrix is equal to the mass of body k , and 3×3 zero matrices $\underline{0}$. The quantity \mathcal{V}_0^k is the 6×1 absolute spatial velocity associated with the center of mass of body k . This matrix comprises of the 3×1 absolute angular velocity vector ω^k of body k and the absolute translational velocity v_0^k of the body k mass center.

For the purpose of making the development which follows clear and concise, the treatment will be limited to multi-rigid body systems. This method may be easily extended to model transitions which include other model types such as flexible bodies, using the development presented in [25]. Additionally, in the analytical treatment presented here, direction cosine matrices and transformations between different basis are not shown explicitly. Appropriate basis transformations have to be taken into account for an implementation of this algorithm. Further, similar to prior multibody literature [26, 27], this algorithm uses a redundant mixed set of coordinates, viz. Cartesian coordinates and relative coordinates, throughout the derivation.

3 Two handle generalized inertia

Consider two representative bodies, body k and body $k + 1$, of any articulated system as shown in Fig. 1. The joint between body k and body $k + 1$ is referred to as J^k . The two handles on body k corresponding to the locations H_1^k and H_2^k are associated with joints J^{k-1} and J^k respectively. Similarly, the two handles on body $k + 1$ corresponding to the locations H_1^{k+1} and H_2^{k+1} are associated with joints J^k and J^{k+1} . Further the velocities of the handles H_1^k and H_2^k and the constraint loads acting on these points will be denoted by the superscript k and subscripts 1 and 2, respectively.

For notational convenience, let the subscript t^- and t^+ represent the state of any quantity before and after, respectively, of an event. For example, let the spatial velocity \mathcal{V}_0^k before an event be represented as \mathcal{V}_{0,t^-}^k while after an event it is represented as \mathcal{V}_{0,t^+}^k .

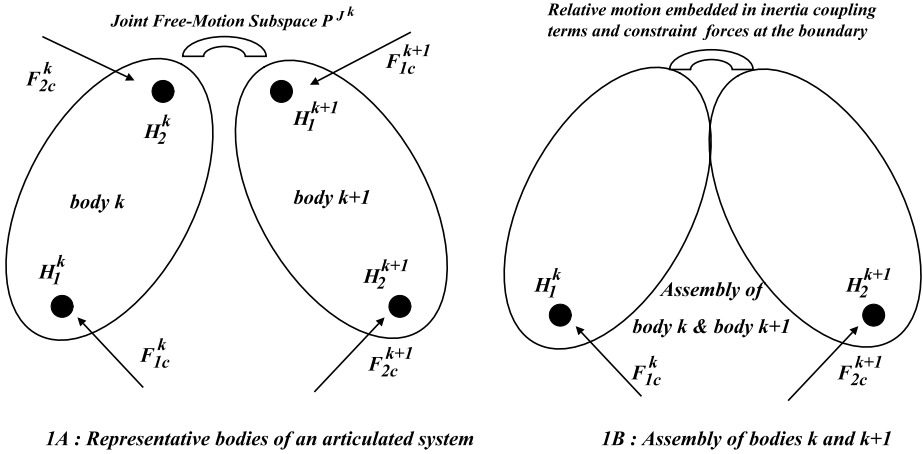


Fig. 1 Two representative bodies

Let us consider an example of an event to be a transition between joint models where the joint definition is instantaneously altered. To alter a joint definition, a joint degree of freedom may be constrained out, its line of action may be modified, or additional degrees of freedom may be added (i.e., the breaking of a prior joint constraint). In any regard the joint definition is instantaneously altered.

The altering of the joint definition can be analytically modeled as the change in the joint free-motion map. Consider for example a spherical joint being altered. Before the event, the joint free-motion map of the spherical joint is $P_{t^-}^{J^k}$ as shown in (5). As before, the joint definition can be altered in a number of ways. If the joint is fully locked out, there are no relative degrees of freedom remaining in the joint and its new joint free-motion map is a null matrix. On the other hand, if only a single degree of freedom is constrained, say the rotation about the second joint axis is constrained, the new joint free-motion map is given by $P_{t^+}^{J^k}$ in (5)

$$P_{t^-}^{J^k} = \begin{bmatrix} 1 & 0 & 0 \\ 0 & 1 & 0 \\ 0 & 0 & 1 \\ 0 & 0 & 0 \\ 0 & 0 & 0 \\ 0 & 0 & 0 \end{bmatrix}, \quad P_{t^+}^{J^k} = \begin{bmatrix} 1 & 0 \\ 0 & 0 \\ 0 & 1 \\ 0 & 0 \\ 0 & 0 \\ 0 & 0 \end{bmatrix}. \tag{5}$$

It is apparent that when the joint definition is altered during an event, the number of generalized speeds, u , across a joint changes. For example, if the joint is fully locked out, the number of generalized speeds become zero while for the case shown in (5), the number of generalized speeds changes from 3 to 2.

For this derivation, let us differentiate between the terminology of altered and unaltered joints. Altered joints are those where the joint definitions have been changed instantaneously resulting in specific generalized speeds being instantaneously constrained. The unaltered joints are the ones where the joint definition is not changed.

In either of these cases, the spatial impulse–momentum equations of a representative body k about its center of mass can be written as below with \underline{U} being a 3×3 identity matrix

and $(r^{k_i/k_j}) \times$ being the 3×3 skew symmetric matrix of the position vector (r^{k_i/k_j}) .

$$\mathcal{L}_{0t^+}^k - \mathcal{L}_{0t^-}^k = \int_{t^-}^{t^+} \mathcal{F}_0^k dt \tag{6}$$

$$\begin{aligned} \Rightarrow \mathcal{L}_{0t^+}^k - \mathcal{L}_{0t^-}^k &= \int_{t^-}^{t^+} \mathcal{S}^{k_1/k_0} \mathcal{F}_{c_1}^k dt \\ &+ \int_{t^-}^{t^+} \mathcal{S}^{k_2/k_0} \mathcal{F}_{c_2}^k dt + \int_{t^-}^{t^+} \mathcal{F}_a^k dt + \underbrace{\int_{t^-}^{t^+} \mathcal{F}_{\text{non}}^k dt}_0 \end{aligned} \tag{7}$$

with

$$\mathcal{L}_0^k = \begin{bmatrix} I_0^k \omega_0^k \\ m^k v_0^k \end{bmatrix} = \begin{bmatrix} I_0^k & \underline{0} \\ \underline{0} & m^k \end{bmatrix} \begin{bmatrix} \omega_0^k \\ v_0^k \end{bmatrix} \tag{8}$$

where

$$\mathcal{L}_{0t^+}^k - \mathcal{L}_{0t^-}^k = \mathcal{M}_0^k [\mathcal{V}_{0t^+}^k - \mathcal{V}_{0t^-}^k] = \mathcal{M}_0^k \Delta \mathcal{V}_0^k \tag{9}$$

and

$$\mathcal{S}^{k_0/k_1} = \begin{bmatrix} \underline{U} & (r^{k_0/k_1}) \times \\ \underline{0} & \underline{U} \end{bmatrix}, \quad \mathcal{S}^{k_0/k_2} = \begin{bmatrix} \underline{U} & (r^{k_0/k_2}) \times \\ \underline{0} & \underline{U} \end{bmatrix}. \tag{10}$$

In the above, \mathcal{F}_0^k is the effective equivalent spatial impulsive load acting on body k at its center of mass. This load is the sum of the impulsive constraint force acting on body k at its inward handle i.e point k_1 represented by $\int_{t^-}^{t^+} \mathcal{F}_{c_1}^k dt$, and the impulsive constraint force acting at its outward handle i.e. point k_2 represented by $\int_{t^-}^{t^+} \mathcal{F}_{c_2}^k dt$, while the active impulsive loads acting on the body at its center of mass represented by the term $\int_{t^-}^{t^+} \mathcal{F}_a^k dt$. The term $\int_{t^-}^{t^+} \mathcal{F}_{\text{non}}^k dt$ represents the effect of all nonimpulsive loads acting on the body. These loads include nonimpulsive spatial active loads such as actuators, spring forces and forces arising from potential fields. The effect of nonimpulsive forces over the duration of the event is negligible and hence is represented in the above equation as zero.

In the equations, although the term $\int_{t^-}^{t^+} \mathcal{F}_a^k dt$ has been explicitly shown, in applications discussed here, this term is absent because there are no externally applied impulsive forces being explicitly applied to the bodies. This term needs to be accounted for in cases when an event is being studied using a contact model and not through a joint. This quantity is state dependent and can be calculated upfront using either a coefficient of restitution model, or some other pertinent contact model in appropriate applications. In any case, the term is either zero or considered to be a state dependent known quantity.

The change in spatial momentum of any body can also be written in terms of the velocities of the two handles on the body by using the kinematic relation between the spatial velocities of the center of mass and the handles. In these equations, the term $\Delta \mathcal{V}$ indicates a jump in the spatial velocity of a body. The jump reflects a discontinuous change in the value of the spatial velocities arising from an event.

$$\mathcal{L}_{0t^+}^k - \mathcal{L}_{0t^-}^k = \mathcal{M}_0^k [\mathcal{V}_{0t^+}^k - \mathcal{V}_{0t^-}^k] = \mathcal{M}_0^k (\mathcal{S}^{k_0/k_1})^T [\mathcal{V}_{1t^+}^k - \mathcal{V}_{1t^-}^k] = \mathcal{M}_0^k (\mathcal{S}^{k_0/k_1})^T \Delta \mathcal{V}_1^k, \tag{11}$$

$$\mathcal{L}_{0t^+}^k - \mathcal{L}_{0t^-}^k = \mathcal{M}_0^k [\mathcal{V}_{0t^+}^k - \mathcal{V}_{0t^-}^k] = \mathcal{M}_0^k (\mathcal{S}^{k_0/k_2})^T [\mathcal{V}_{2t^+}^k - \mathcal{V}_{2t^-}^k] = \mathcal{M}_0^k (\mathcal{S}^{k_0/k_2})^T \Delta \mathcal{V}_2^k. \tag{12}$$

Thus combining the above equations (7–11), the impulse–momentum equations for body k can be written in terms of the velocity jump at handle 1 as

$$\mathcal{M}_0^k (\mathcal{S}^{k_0/k_1})^T \Delta \mathcal{V}_1^k = \int_{t^-}^{t^+} \mathcal{S}^{k_1/k_0} \mathcal{F}_{c_1}^k dt + \int_{t^-}^{t^+} \mathcal{S}^{k_2/k_0} \mathcal{F}_{c_2}^k dt + \int_{t^-}^{t^+} \mathcal{F}_a^k dt \quad (13)$$

$$\Rightarrow \Delta \mathcal{V}_1^k = \Phi_{11}^k \int_{t^-}^{t^+} \mathcal{F}_{c_1}^k dt + \Phi_{12}^k \int_{t^-}^{t^+} \mathcal{F}_{c_2}^k dt + \Phi_{13}^k. \quad (14)$$

In a similar fashion, the impulse–momentum equation for body k can be written in terms of the velocity jump at handle 2 as

$$\mathcal{M}_0^k (\mathcal{S}^{k_0/k_2})^T \Delta \mathcal{V}_2^k = \int_{t^-}^{t^+} \mathcal{S}^{k_1/k_0} \mathcal{F}_{c_1}^k dt + \int_{t^-}^{t^+} \mathcal{S}^{k_2/k_0} \mathcal{F}_{c_2}^k dt + \int_{t^-}^{t^+} \mathcal{F}_a^k dt \quad (15)$$

$$\Rightarrow \Delta \mathcal{V}_2^k = \Phi_{21}^k \int_{t^-}^{t^+} \mathcal{F}_{c_1}^k dt + \Phi_{22}^k \int_{t^-}^{t^+} \mathcal{F}_{c_2}^k dt + \Phi_{23}^k. \quad (16)$$

The impulse–momentum equation of the body k when referred to the jump in the velocities of the two handles on the body will henceforth be referred to as the two handle impulse–momentum equations as shown in (17, 18).

$$\Delta \mathcal{V}_1^k = \Phi_{11}^k \int_{t^-}^{t^+} \mathcal{F}_{c_1}^k dt + \Phi_{12}^k \int_{t^-}^{t^+} \mathcal{F}_{c_2}^k dt + \Phi_{13}^k, \quad (17)$$

$$\Delta \mathcal{V}_2^k = \Phi_{21}^k \int_{t^-}^{t^+} \mathcal{F}_{c_1}^k dt + \Phi_{22}^k \int_{t^-}^{t^+} \mathcal{F}_{c_2}^k dt + \Phi_{23}^k. \quad (18)$$

Similarly, the two handle impulse–momentum equations for body $k + 1$ can also be written in the same fashion as below

$$\Delta \mathcal{V}_1^{k+1} = \Phi_{11}^{k+1} \int_{t^-}^{t^+} \mathcal{F}_{c_1}^{k+1} dt + \Phi_{12}^{k+1} \int_{t^-}^{t^+} \mathcal{F}_{c_2}^{k+1} dt + \Phi_{13}^{k+1}, \quad (19)$$

$$\Delta \mathcal{V}_2^{k+1} = \Phi_{21}^{k+1} \int_{t^-}^{t^+} \mathcal{F}_{c_1}^{k+1} dt + \Phi_{22}^{k+1} \int_{t^-}^{t^+} \mathcal{F}_{c_2}^{k+1} dt + \Phi_{23}^{k+1}. \quad (20)$$

Now consider the relative velocity at the intermediate joint between the two bodies. The joint free-motion map for this joint is given by P^{J^k} . From the definition of the joint free-motion map, the following kinematic relation exists.

$$\mathcal{V}_1^{k+1} - \mathcal{V}_2^k = P^{J^k} u^{k/k+1} \quad (21)$$

$$\Rightarrow \Delta \mathcal{V}_1^{k+1} - \Delta \mathcal{V}_2^k = \Delta(P^{J^k} u^{k/k+1}). \quad (22)$$

In the above equations, the term $\Delta(P^{J^k} u^{k/k+1})$ accounts for the instantaneous changes across the joint. If the joint is an unaltered type, the joint free-motion map is not changed and hence the term becomes

$$\Delta(P^{J^k} u^{k/k+1}) = P^{J^k} [u_{t^+}^{k/k+1} - u_{t^-}^{k/k+1}] = P^{J^k} \Delta u^{k/k+1} \quad (23)$$

where $\Delta u^{k/k+1}$ is the jump in the generalized speeds across the joint associated with a discontinuous change or event.

However, if the joint is the altered one, then there is an instantaneous change in the joint free-motion map as well as the values of the generalized speeds. The term $\Delta(P^{J^k} u^{k/k+1})$ becomes

$$\Delta(P^{J^k} u^{k/k+1}) = P_{t^+}^{J^k} u_{t^+}^{k/k+1} - P_{t^-}^{J^k} u_{t^-}^{k/k+1}. \tag{24}$$

In both the above equations (23, 24), the only unknown in either case is the term $u_{t^+}^{k/k+1}$. The generalized speed before the event $u_{t^-}^{k/k+1}$ as well as the joint free-motion maps before $P_{t^-}^{J^k}$ and after $P_{t^+}^{J^k}$ the event are known quantities. Also, in the two handle equations (17, 18), the constraint impulsive forces at either handle are the unknown quantities.

From Newton’s third law of motion, the impulsive loads acting on either body at the intermediate joint are equal in magnitude and opposite in direction, i.e.,

$$\int_{t^-}^{t^+} \mathcal{F}_{c_2}^k dt = - \int_{t^-}^{t^+} \mathcal{F}_{c_1}^{k+1} dt. \tag{25}$$

Substituting the expressions for $\Delta \mathcal{V}_2^k$ and $\Delta \mathcal{V}_1^{k+1}$ from (18) and (19), respectively, into the kinematic relation given by (22) and using the relation between the constraint forces from above equation (25), the following expressions can be obtained:

$$\begin{aligned} \Delta(P^{J^k} u^{k/k+1}) &= \Phi_{11}^{k+1} \int_{t^-}^{t^+} \mathcal{F}_{c_1}^{k+1} dt + \Phi_{12}^{k+1} \int_{t^-}^{t^+} \mathcal{F}_{c_2}^{k+1} dt + \Phi_{13}^{k+1} \\ &\quad - \Phi_{21}^k \int_{t^-}^{t^+} \mathcal{F}_{c_1}^k dt - \Phi_{22}^k \int_{t^-}^{t^+} \mathcal{F}_{c_2}^k dt - \Phi_{23}^k \tag{26} \\ \Rightarrow [\Phi_{22}^k + \Phi_{11}^{k+1}] \int_{t^-}^{t^+} \mathcal{F}_{c_1}^{k+1} dt &= \Phi_{21}^k \int_{t^-}^{t^+} \mathcal{F}_{c_1}^k dt + \Phi_{23}^k \\ &\quad - \Phi_{12}^{k+1} \int_{t^-}^{t^+} \mathcal{F}_{c_2}^{k+1} dt - \Phi_{13}^{k+1} \\ &\quad + \Delta(P^{J^k} u^{k/k+1}). \tag{27} \end{aligned}$$

In the above equation, the constraint impulsive loads at the common joint is expressed in terms of the constraint impulsive loads at the other two handles on the two bodies and the incremental jump in the relative spatial velocity across the joint. However, the objective is to decouple the constraint impulsive loads from the jump in the generalized speeds. To do this, the space in which the spatial constraint impulses are contained needs to be analyzed.

Irrespective of whether the joint is an altered or an unaltered joint, the spatial constraint impulsive loads lie in exactly the space spanned by the orthogonal complement of the joint free-motion map of the joint after the event, i.e., $D_{t^+}^{J^k}$. As indicated earlier, a kinematic joint can support constraint loads in the space spanned by the orthogonal complement of the joint free-motion map. Now if the joint is unaltered in the event, then the orthogonal complement remains the same and the joint impulsive constraint loads are contained in the space spanned by $D_{t^+}^{J^k} (= D_{t^-}^{J^k})$.

In the case of an altered joint, the constraint impulsive loads lie in the space spanned by the orthogonal complement of the altered joint free-motion map. Consider for example, a joint where one or more relative degrees of freedom are instantaneously suppressed. In terms

of the free-motion map matrices, this means that one or more column matrices of the joint free-motion map are instantaneously eliminated and the same column matrices are appended to the orthogonal complement matrix. Clearly the constraint impulses applied at the joint to suppress the joint degrees of freedom are in the same space spanned by the column matrices that transition from the joint free-motion map to the orthogonal complement matrix. There are also additional constraint impulsive loads acting at the joint due to the coupling with all the other bodies in the system. These constraint impulsive loads are contained in the space where the joint can no longer allow relative motion, i.e., the space spanned by the orthogonal complement of the joint free-motion map after the event $D_{i+}^{J^k}$. A joint definition may also be altered in cases where additional degrees of freedom at a joint become active, or cases where the line of action of a joint is modified without changing the number of degrees of freedom, among other instances. In such cases too, the constraint impulsive loads as shown in (27) are contained in the space spanned by the orthogonal complement of the joint free-motion map after the event, i.e., $D_{i+}^{J^k}$.

Hence, to eliminate the jump in the generalized speeds from (27), pre-multiply (27) by $[D_{i+}^{J^k}]^T$. By the definition of orthogonality, $(D_{i+}^{J^k})^T P_{i+}^{J^k} = 0$ and hence the jump in the relative spatial velocity is now eliminated from the equation. Further, the spatial constraint impulses are contained in the space mapped by the orthogonal complement of the joint free-motion map. Hence the spatial constraint impulses can be expressed in terms of the measure numbers of the constraint impulsive loads. Here \mathbf{F} is an order list of the measure numbers of the constraint torques and forces.

$$\int_{t-}^{t+} \mathcal{F}_{c_1}^{k+1} dt = D_{i+}^{J^k} \int_{t-}^{t+} \mathbf{F}_{c_1}^{k+1} dt. \tag{28}$$

Substituting this expression into above equation (27) and multiplying by $[D_{i+}^{J^k}]^T$, the desired expression for the constraint impulsive loads at the common joint can be obtained as

$$\begin{aligned} & [D_{i+}^{J^k}]^T [\Phi_{22}^k + \Phi_{11}^{k+1}] D_{i+}^{J^k} \int_{t-}^{t+} \mathbf{F}_{c_1}^{k+1} dt \\ &= [D_{i+}^{J^k}]^T \Phi_{21}^k \int_{t-}^{t+} \mathcal{F}_{c_1}^k dt + [D_{i+}^{J^k}]^T \Phi_{23}^k - [D_{i+}^{J^k}]^T \Phi_{12}^{k+1} \int_{t-}^{t+} \mathcal{F}_{c_2}^{k+1} dt \\ &\quad - [D_{i+}^{J^k}]^T \Phi_{13}^{k+1} + \underbrace{[D_{i+}^{J^k}]^T P_{i+}^{J^k} u_{i+}^{k/k+1}}_0 - [D_{i+}^{J^k}]^T P_{i-}^{J^k} u_{i-}^{k/k+1} \end{aligned} \tag{29}$$

$$\begin{aligned} \Rightarrow \int_{t-}^{t+} \mathcal{F}_{c_1}^{k+1} dt &= D_{i+}^{J^k} ([D_{i+}^{J^k}]^T [\Phi_{22}^k + \Phi_{11}^{k+1}] D_{i+}^{J^k})^{-1} [D_{i+}^{J^k}]^T \left\{ \Phi_{21}^k \int_{t-}^{t+} \mathcal{F}_{c_1}^k dt \right. \\ &\quad \left. + \Phi_{23}^k - \Phi_{12}^{k+1} \int_{t-}^{t+} \mathcal{F}_{c_2}^{k+1} dt - \Phi_{13}^{k+1} - P_{i-}^{J^k} u_{i-}^{k/k+1} \right\} \end{aligned} \tag{30}$$

$$\Rightarrow \int_{t-}^{t+} \mathcal{F}_{c_1}^{k+1} dt = \mathcal{X} \Phi_{21}^k \int_{t-}^{t+} \mathcal{F}_{c_1}^k dt - \mathcal{X} \Phi_{12}^{k+1} \int_{t-}^{t+} \mathcal{F}_{c_2}^{k+1} dt + \mathcal{Y}, \tag{31}$$

$$\text{where } \mathcal{X} = D_{i+}^{J^k} ([D_{i+}^{J^k}]^T [\Phi_{22}^k + \Phi_{11}^{k+1}] D_{i+}^{J^k})^{-1} [D_{i+}^{J^k}]^T, \tag{32}$$

$$\text{and } \mathcal{Y} = \mathcal{X} [\Phi_{23}^k - \Phi_{13}^{k+1} - P_{i-}^{J^k} u_{i-}^{k/k+1}]. \tag{33}$$

The above expression for the constraint impulses at the common joint can be substituted into the corresponding two handle impulse–momentum equations at the other two handles of the

bodies and after some manipulations can be obtained as below:

$$\Delta \mathcal{V}_1^k = [\Phi_{11}^k - \Phi_{12}^k \mathcal{X} \Phi_{21}^k] \int_{t^-}^{t^+} \mathcal{F}_{c_1}^k dt + [\Phi_{12}^k \mathcal{X} \Phi_{12}^{k+1}] \int_{t^-}^{t^+} \mathcal{F}_{c_2}^{k+1} dt + [\Phi_{13}^k - \Phi_{12}^k \mathcal{Y}] \quad (34)$$

$$\begin{aligned} \text{and } \Delta \mathcal{V}_2^{k+1} &= [\Phi_{21}^{k+1} \mathcal{X} \Phi_{21}^k] \int_{t^-}^{t^+} \mathcal{F}_{c_1}^k dt \\ &+ [\Phi_{22}^{k+1} - \Phi_{21}^{k+1} \mathcal{X} \Phi_{12}^{k+1}] \mathcal{F}_{c_2}^{k+1} dt + [\Phi_{23}^{k+1} + \Phi_{21}^{k+1} \mathcal{Y}]. \end{aligned} \quad (35)$$

In the above equations, the spatial impulse–momentum equations of body k and body $k + 1$ are coupled together to form the corresponding equations of the assembly of bodies k and $k + 1$ represented as $k : k + 1$. For the assembly, $\Delta \mathcal{V}_1^{k:k+1}$ and $\Delta \mathcal{V}_2^{k:k+1}$ represent the jumps in the spatial velocities at its boundary joints. Collecting terms in above equations, the equations of the assembly can be written as

$$\Delta \mathcal{V}_1^{k:k+1} = \Upsilon_{11}^{k:k+1} \int_{t^-}^{t^+} \mathcal{F}_{c_1}^{k:k+1} dt + \Upsilon_{12}^{k:k+1} \int_{t^-}^{t^+} \mathcal{F}_{c_2}^{k:k+1} dt + \Upsilon_{13}^{k:k+1}, \quad (36)$$

$$\Delta \mathcal{V}_2^{k:k+1} = \Upsilon_{21}^{k:k+1} \int_{t^-}^{t^+} \mathcal{F}_{c_1}^{k:k+1} dt + \Upsilon_{22}^{k:k+1} \int_{t^-}^{t^+} \mathcal{F}_{c_2}^{k:k+1} dt + \Upsilon_{23}^{k:k+1}. \quad (37)$$

The above equations (36, 37) can be considered as the two handle impulse–momentum equations of the resulting assembly of body k and body $k + 1$. From the above, a recursive set of expressions for the inertia coupling terms of the resulting assembly $\Upsilon_{ij}^{k:k+1}$ can be obtained as follows below:

$$\Upsilon_{11}^{k:k+1} = [\Phi_{11}^k - \Phi_{12}^k \mathcal{X} \Phi_{21}^k], \quad (38)$$

$$\Upsilon_{12}^{k:k+1} = [\Phi_{12}^k \mathcal{X} \Phi_{12}^{k+1}], \quad (39)$$

$$\Upsilon_{13}^{k:k+1} = [\Phi_{13}^k - \Phi_{12}^k \mathcal{Y}], \quad (40)$$

$$\Upsilon_{21}^{k:k+1} = [\Phi_{21}^{k+1} \mathcal{X} \Phi_{21}^k], \quad (41)$$

$$\Upsilon_{22}^{k:k+1} = [\Phi_{22}^{k+1} - \Phi_{21}^{k+1} \mathcal{X} \Phi_{12}^{k+1}], \quad (42)$$

$$\Upsilon_{23}^{k:k+1} = [\Phi_{23}^{k+1} + \Phi_{21}^{k+1} \mathcal{Y}]. \quad (43)$$

4 Hierarchic assembly–disassembly

In the previous section, a set of recursive formulae are derived that are used to couple together the spatial impulse–momentum equations of two consecutive bodies to form the corresponding equations of the resulting assembly. In the associated manipulations, the two bodies are coupled together to form an assembly by expressing the intermediate (common) joint constraint impulsive loads in terms of the spatial constraint impulsive loads at the other two handles and the inertia coupling terms. This process can now be repeated for all bodies in the system where the spatial impulse–momentum equations of two successive bodies or assemblies are coupled together using the recursive formulae to obtain the corresponding equations of the resulting assembly. It is similar to the divide and conquer scheme for

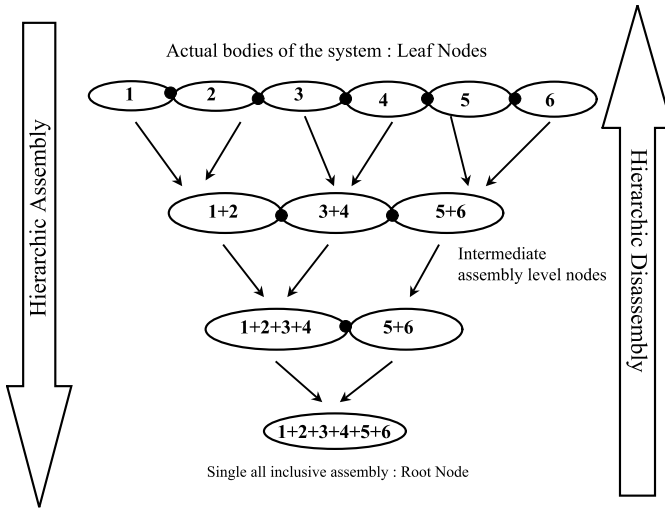


Fig. 2 The hierarchic assembly and disassembly process using binary tree structure

solving the equations of motion of rigid bodies [22, 23]. This process works hierarchically exploiting the same structure as that of a binary tree.

The hierarchic assembly process begins at the level of individual bodies of the system. Adjacent bodies of the system are hierarchically assembled to construct a binary tree as shown in Fig. 2. Individual bodies that make up the system form the leaf nodes of the binary tree. The impulse–momentum equations of a pair of bodies are coupled together using the recursive set of formulae to form the corresponding equations of the resulting assembly. The resulting assembly now corresponds to a node of the next level in the binary tree. Working along the binary tree in this hierarchic assembly processes, only a single assembly is left as the root node of the binary tree. The root node corresponds to the two-handle representation of the entire articulated system modeled as a single assembly. The impulse–momentum equations of this root node can be expressed as

$$\Delta \mathcal{V}_1^{1:n} = \Phi_{11}^{1:n} \int_{t^-}^{t^+} \mathcal{F}_{c_1}^{1:n} dt + \Phi_{12}^{1:n} \int_{t^-}^{t^+} \mathcal{F}_{c_2}^{1:n} dt + \Phi_{13}^{1:n}, \tag{44}$$

$$\Delta \mathcal{V}_2^{1:n} = \Phi_{21}^{1:n} \int_{t^-}^{t^+} \mathcal{F}_{c_1}^{1:n} dt + \Phi_{22}^{1:n} \int_{t^-}^{t^+} \mathcal{F}_{c_2}^{1:n} dt + \Phi_{23}^{1:n}. \tag{45}$$

Here the superscript 1 : n is used to denote the whole system being represented as a single assembly as the root node of the binary tree. In this case, the handles 1 and 2 of this entity are the boundary joints of the articulated system. Similarly the spatial constraint impulsive loads are those arising from the interaction of the system with its boundaries. The above represent two sets of equations in terms of four sets of unknowns, i.e., the jumps in the spatial velocities at the boundary joints $\Delta \mathcal{V}_1^{1:n}$, $\Delta \mathcal{V}_2^{1:n}$ and the corresponding constraint impulsive loads and $\int_{t^-}^{t^+} \mathcal{F}_{c_1}^{1:n} dt$, $\int_{t^-}^{t^+} \mathcal{F}_{c_2}^{1:n} dt$. Consider the three following scenarios that may arise for a system.

4.1 Free floating

This case corresponds to a system which is free floating, i.e., there are no kinematic joints connecting the system to the inertial frame. In the absence of any kinematic joints at either boundary, there are no constraint impulses that can act on the system at the boundaries. In this case, in (44, 45) the constraint impulse terms are all zero and the jumps in the spatial velocities can be easily solved as

$$\Delta \mathcal{V}_1^{1:n} = \Phi_{13}^{1:n}, \tag{46}$$

$$\Delta \mathcal{V}_2^{1:n} = \Phi_{23}^{1:n}. \tag{47}$$

4.2 Anchored at one end by kinematic joint

In this case, the system is connected to the inertial frame by a kinematic joint at one end while the other end is free floating. For such a system, there are no constraint impulsive loads acting at the free end and in (44, 45) the term $\int_{t^-}^{t^+} \mathcal{F}_{c_2}^{1:n} dt = 0$. However at the connected end, the system will experience a constraint impulsive loads because of the kinematic joint. The spatial impulse–momentum equations in this case reduce to

$$\Delta \mathcal{V}_1^{1:n} = \Phi_{11}^{1:n} \int_{t^-}^{t^+} \mathcal{F}_{c_1}^{1:n} dt + \Phi_{13}^{1:n}, \tag{48}$$

$$\Delta \mathcal{V}_2^{1:n} = \Phi_{21}^{1:n} \int_{t^-}^{t^+} \mathcal{F}_{c_1}^{1:n} dt + \Phi_{23}^{1:n}. \tag{49}$$

From the definition of the kinematic joint and its joint free-motion map, there exist the following kinematic relations:

$$\mathcal{V}_1^{1:n} = P^1 u^1 \tag{50}$$

$$\Rightarrow \Delta \mathcal{V}_1^{1:n} = \Delta(P^1 u^1). \tag{51}$$

Further, from the definition of the orthogonal complement of the joint free-motion map, the constraint impulses at the handle can be expressed as

$$\int_{t^-}^{t^+} \mathcal{F}_{c_1}^{1:n} dt = D_{t^+}^1 \int_{t^-}^{t^+} \mathbf{F}_{c_1}^{1:n} dt. \tag{52}$$

Substituting the above equations (51, 52) into (48, 49), the following is obtained:

$$\Delta(P^1 u^1) = P_{t^+}^1 u_{t^+}^1 - P_{t^-}^1 u_{t^-}^1 = \Phi_{11}^{1:n} D_{t^+}^1 \int_{t^-}^{t^+} \mathbf{F}_{c_1}^{1:n} dt + \Phi_{13}^{1:n} \tag{53}$$

$$\Rightarrow P_{t^+}^1 u_{t^+}^1 = \Phi_{11}^{1:n} D_{t^+}^1 \int_{t^-}^{t^+} \mathbf{F}_{c_1}^{1:n} dt + \Phi_{13}^{1:n} + P_{t^-}^1 u_{t^-}^1. \tag{54}$$

Using the orthogonality relation between $P_{t^+}^1$ and $D_{t^+}^1$, the new generalized speed at the joint as well as the constraint impulsive loads can be solved from (54) as

$$\int_{t^-}^{t^+} \mathcal{F}_{c_1}^{1:n} dt = -D_{t^+}^1 [(D_{t^+}^1)^T \Phi_{11}^{1:n} D_{t^+}^1]^{-1} (D_{t^+}^1)^T [\Phi_{13}^{1:n} + P_{t^-}^1 u_{t^-}^1], \tag{55}$$

$$u_{t^+}^1 = P_{t^+}^1 [(P_{t^+}^1)^T (\Phi_{11}^{1:n})^{-1} P_{t^+}^1]^{-1} (P_{t^+}^1)^T [\Phi_{13}^{1:n} + P_{t^-}^1 u_{t^-}^1]. \tag{56}$$

Substituting the above equations (55, 56) into (48, 49), the jumps in the boundary spatial velocities, i.e., $\Delta \mathcal{V}_1^{1:n}$ and $\Delta \mathcal{V}_1^{2:n}$ can be easily calculated.

4.3 Anchored at both ends by kinematic joints

In this case, the system is connected to the inertial frame by kinematic joints at both ends. Here, the system reduces to a kinematically closed loop topology. For such a system, there are constraint impulsive loads acting at both the ends due to the kinematic joints. In this case, the spatial impulse–momentum equation for the system is

$$\Delta \mathcal{V}_1^{1:n} = \Phi_{11}^{1:n} \int_{t-}^{t+} \mathcal{F}_{c_1}^{1:n} dt + \Phi_{12}^{1:n} \int_{t-}^{t+} \mathcal{F}_{c_2}^{1:n} dt + \Phi_{13}^{1:n}, \tag{57}$$

$$\Delta \mathcal{V}_2^{1:n} = \Phi_{21}^{1:n} \int_{t-}^{t+} \mathcal{F}_{c_1}^{1:n} dt + \Phi_{22}^{1:n} \int_{t-}^{t+} \mathcal{F}_{c_2}^{1:n} dt + \Phi_{23}^{1:n}. \tag{58}$$

Similar to the previous situation, the following kinematic relations exist between the boundary joints and their joint free-motion maps.

$$\mathcal{V}_1^{1:n} = P^1 u^1 \quad \text{and} \quad \mathcal{V}_2^{1:n} = P^2 u^2 \tag{59}$$

$$\Rightarrow \Delta \mathcal{V}_1^{1:n} = \Delta(P^1 u^1) \quad \text{and} \quad \Delta \mathcal{V}_2^{1:n} = \Delta(P^2 u^2). \tag{60}$$

Further, from the definition of the orthogonal complement of the joint free-motion map, the constraint impulses at the handle can be expressed as

$$\int_{t-}^{t+} \mathcal{F}_{c_1}^{1:n} dt = D_{t+}^1 \int_{t-}^{t+} \mathbf{F}_{c_1}^{1:n} dt \quad \text{and} \quad \int_{t-}^{t+} \mathcal{F}_{c_2}^{1:n} dt = D_{t+}^2 \int_{t-}^{t+} \mathbf{F}_{c_2}^{1:n} dt. \tag{61}$$

Substituting (60) into (57, 58) and absorbing the terms $(P^i u^i)_{t-}$ into the $\Phi_{i3}^{1:n}$ ($i = 1, 2$), one obtains,

$$P_{t+}^1 u_{t+}^1 = \Phi_{11}^{1:n} \int_{t-}^{t+} \mathcal{F}_{c_1}^{1:n} dt + \Phi_{12}^{1:n} \int_{t-}^{t+} \mathcal{F}_{c_2}^{1:n} dt + \Phi_{13}^{1:n}, \tag{62}$$

$$P_{t+}^2 u_{t+}^2 = \Phi_{21}^{1:n} \int_{t-}^{t+} \mathcal{F}_{c_1}^{1:n} dt + \Phi_{22}^{1:n} \int_{t-}^{t+} \mathcal{F}_{c_2}^{1:n} dt + \Phi_{23}^{1:n}. \tag{63}$$

Multiplying the above equations by $(D_{t+}^1)^T$ and $(D_{t+}^2)^T$ respectively, and calling on the orthogonality relation, the following is obtained.

$$\overbrace{(D_{t+}^1)^T P_{t+}^1 u_{t+}^1}^0 = (D_{t+}^1)^T \left[\Phi_{11}^{1:n} \int_{t-}^{t+} \mathcal{F}_{c_1}^{1:n} dt + \Phi_{12}^{1:n} \int_{t-}^{t+} \mathcal{F}_{c_2}^{1:n} dt + \Phi_{13}^{1:n} \right] = 0, \tag{64}$$

$$\overbrace{(D_{t+}^2)^T P_{t+}^2 u_{t+}^2}^0 = (D_{t+}^2)^T \left[\Phi_{21}^{1:n} \int_{t-}^{t+} \mathcal{F}_{c_1}^{1:n} dt + \Phi_{22}^{1:n} \int_{t-}^{t+} \mathcal{F}_{c_2}^{1:n} dt + \Phi_{23}^{1:n} \right] = 0. \tag{65}$$

Substituting the expressions for the constraint impulse from (61) into (64, 65) one obtains

$$(D_{t+}^1)^T \Phi_{11}^{1:n} D_{t+}^1 \int_{t-}^{t+} \mathbf{F}_{c_1}^{1:n} dt + (D_{t+}^1)^T \Phi_{12}^{1:n} D_{t+}^2 \int_{t-}^{t+} \mathbf{F}_{c_2}^{1:n} dt + (D_{t+}^2)^T \Phi_{13}^{1:n} = 0, \tag{66}$$

$$(D_{t^+}^2)^T \Phi_{21}^{1:n} D_{t^+}^1 \int_{t^-}^{t^+} \mathbf{F}_{c_1}^{1:n} dt + (D_{t^+}^2)^T \Phi_{22}^{1:n} D_{t^+}^2 \int_{t^-}^{t^+} \mathbf{F}_{c_2}^{1:n} dt + (D_{t^+}^2)^T \Phi_{23}^{1:n} = 0. \tag{67}$$

In these equations, the terms $(D_{t^+}^1)^T \Phi_{11}^{1:n} D_{t^+}^1$ and $(D_{t^+}^2)^T \Phi_{22}^{1:n} D_{t^+}^2$ are symmetric positive definite (SPD) matrices and there is no problem associated with their inversion. For notational convenience, the above equations can be represented compactly in matrix form as

$$\begin{bmatrix} \chi_{11} & \chi_{12} \\ \chi_{21} & \chi_{22} \end{bmatrix} \begin{bmatrix} \int_{t^-}^{t^+} \mathbf{F}_{c_1}^{1:n} dt \\ \int_{t^-}^{t^+} \mathbf{F}_{c_2}^{1:n} dt \end{bmatrix} = - \begin{bmatrix} \chi_{13} \\ \chi_{23} \end{bmatrix} \tag{68}$$

where the corresponding χ_{ij} can be derived from above equations. The matrix in (68) is SPD with $\chi_{12} = \chi_{21}^T$ and hence the set of equations can be easily solved. Having solved the above equations for the values of $\int_{t^-}^{t^+} \mathbf{F}_{c_1}^{1:n} dt$ and $\int_{t^-}^{t^+} \mathbf{F}_{c_2}^{1:n} dt$, the corresponding expression for $\int_{t^-}^{t^+} \mathcal{F}_{c_1}^{1:n} dt$ and $\int_{t^-}^{t^+} \mathcal{F}_{c_2}^{1:n} dt$ can be obtained from (61). At this point, both impulsive constraint loads on the boundary joints are known. Consequently, (57, 58) of the root node can be solved to obtain the jumps in the spatial velocities, i.e., $\Delta \mathcal{V}_1^{1:n}$ and $\Delta \mathcal{V}_2^{1:n}$ at the corresponding joints. This scheme is similar to the [23] for solving the equations of motion of constrained rigid body systems.

Thus in all three cases, the jumps in the spatial velocities and the constraint impulses at the boundary joints can be calculated. This initiates the hierarchic disassembly process. The jumps in the spatial velocities and the constraint impulsive loads generated by solving the spatial impulse–momentum equations of an assembly are identically the values of the jumps in the spatial velocities and the constraint impulsive loads on one handle on each of the two constituent assemblies. From these known quantities, the spatial impulse–momentum equations of the constituent assemblies can be solved to obtain the jumps in the spatial velocities and the constraint impulsive loads at the connecting joint. For example, for a representative assembly made from body k and body $k + 1$, the spatial impulse–momentum equations are given by equations (36, 37). On solving these equations, the quantities $\Delta \mathcal{V}_1^k$, $\Delta \mathcal{V}_2^{k+1}$, $\int_{t^-}^{t^+} \mathcal{F}_{c_1}^k dt$ and $\int_{t^-}^{t^+} \mathcal{F}_{c_2}^{k+1} dt$ are generated. These quantities are then substituted into the spatial impulse–momentum equations of the constituent sub-assemblies for body k and body $k + 1$. Thus knowing the values of $\Delta \mathcal{V}_1^k$, $\int_{t^-}^{t^+} \mathcal{F}_{c_1}^k dt$, (17, 18) can be solved, while from $\Delta \mathcal{V}_2^{k+1}$ and $\int_{t^-}^{t^+} \mathcal{F}_{c_2}^{k+1} dt$ (19, 20) can be solved. This process is repeated in a hierarchic disassembly of the binary tree where the known boundary conditions are used to solve the impulse–momentum equations of the immediate subassemblies, until jumps in the generalized speeds and constraint impulsive loads on all bodies in the system are calculated.

Similar to the scheme in [22, 23], this algorithm works in four sweeps, traversing the system topology like a binary tree. The first and the third sweep work from the leaf nodes of the binary tree to the root node while the second and the fourth sweep work from the root node to the leaf nodes. The input to this algorithm is comprised of the mass properties of the bodies, joint generalized coordinates and speeds. The first two sweeps generate the position and velocity of each handle on each node by using an assembly–disassembly process similar to that described in [22, 23]. The final two sweeps correspond to the hierarchic assembly and the hierarchic disassembly processes, respectively.

4.4 Singular configurations

Modeling systems in kinematically closed loop topologies has traditionally been an interesting problem in multibody dynamics because of the presence of explicit loop closure con-

straints. Along with the dynamics equations of motion of an equivalent unconstrained system, traditional methods maintain the constraints through an extra set of algebraic equations which are used to either (i) reduce out excessive degrees of freedom producing a minimum dimension system of equations; or (ii) augment the equations of motion producing a larger dimension system of equations involving redundant state variables. This gives rise to the saddle point problem originating from constraint equations becoming numerically dependent. When a system enters what is normally called a singular configuration, the constraint equations become numerically dependent and the traditional formulations are unable to solve the governing equations. To circumvent this problem, computationally expensive procedures such as singular value decompositions have to be used to solve the equations. Even if the system is not in a true singular configuration, the equations become significantly ill conditioned and result in significant constraint violation.

However, in the method described in this paper, the loop closure constraint is modeled using a different approach. Instead of using explicit constraint equations, the constraints are implicitly imposed by describing the topology of the system through the relative coordinates and the use of a set of redundant generalized coordinates to enforce the loop closure constraint. The redundant set of generalized coordinates maintains the definition of the kinematic joint that converts an unconstrained system into a constrained system in a loop configuration. The presence of an extra kinematic joint introduces an additional orthogonality relation between the map of the free-motion the joint and its orthogonal complement. This allows for the loop closure constraint to be implicitly imposed. Further, the use of a redundant set of generalized coordinates always maintains the correct dimensionality of the system equations, making this algorithm free from rank deficiency issues as all matrices to be inverted are symmetric positive definite. This ensures that the algorithm can robustly handle what would normally be considered singular configurations. The manner in which this method avoids singularities appears similar, in some regards, to that of Euler parameters. With Euler parameters, one deals with a redundant four-member set of generalized coordinates (parameters) for the global and nonsingular description of general spatial rotation. The constraints between these four coordinates are implicitly enforced. If the constraints were explicitly used to reduce out the extra generalized coordinate (parameter), the representation again may become singular. In the same manner, this algorithm enforces the constraints implicitly thereby avoiding singularities.

It is commonly perceived that singularity is an inherent feature of a system and not just a numerical artifact and hence cannot be circumvented. This is true if the system enters the singular configuration under such conditions that the momentum of the system at the singular configuration is zero. In such a case, there is no unique solution and it represents the inherent singular nature of the system. However, if the system enters the singular configuration with nonzero momentum, the state of the system as it exits the singular configuration is unique and is a function of the momentum of the system. In this case, the singularity is not an inherent feature of the system but rather a numerical artifact observed in most traditional schemes. The algorithm presented here will correctly identify the state of the system as it exits the singular configuration based on the nonzero momentum of the system as it entered the singular configuration.

5 Numerical test cases

Two test cases were simulated using the algorithm to ascertain the validity of the method. This section discusses the details of the test cases, the numerical results obtained and the associated discussion on the performance of the algorithm.

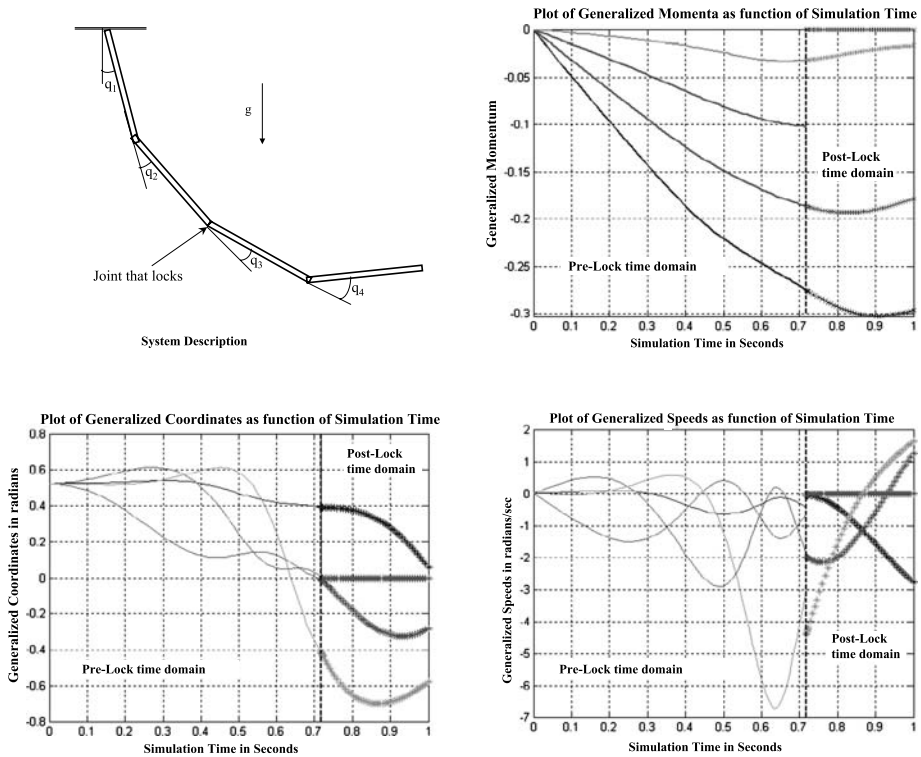


Fig. 3 System with joint lock

5.1 Joint locking

This test case was chosen to validate the ability of the method to simulate systems undergoing *joint locking*, i.e., a system where a joint definition is discontinuously altered. The system under study consists of four rigid bodies with consecutive bodies connected to each other by revolute joints to form a serial chain topology as shown in the Fig. 3. The first body is also connected to the inertial reference frame by a revolute joint. The system is started from rest at the beginning of the simulation and swings freely under the effect of gravity. At a randomly chosen instant, the joint between the second and third body in the system is instantaneously *locked*, i.e., it does not allow any relative motion between the two bodies. This locking of the joints introduces an impulsive load on each body in the system resulting in jumps in the remaining generalized speeds. The system continues to move under the effect of gravity albeit, with a reduced number of degrees of freedom because of the locked joint between bodies two and three.

Each body in the system is modeled as a slender steel bar ($\rho = 7860 \text{ kg/m}^3$) of dimensions $1 \text{ m} \times 1 \text{ mm} \times 1 \text{ mm}$. The simulation is started with all generalized coordinates set at $\pi/3$ and generalized speeds equal to zero. The system moves under gravity for 0.71768 seconds at which point, the joint between bodies 2 and 3 is instantaneously locked. The simulation is then carried on for the modified system for a total simulation time of 1 second. In Fig. 3, the values of the generalized coordinates and speeds of the system are plotted for the duration of the simulation. The instant of the joint locking is shown explicitly.

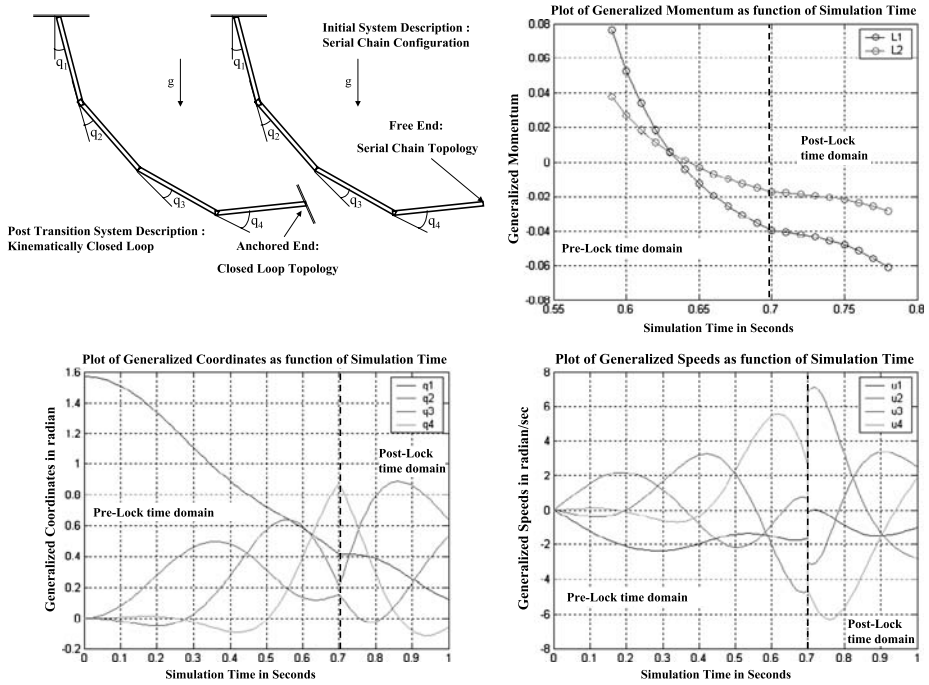


Fig. 4 System with joint lock

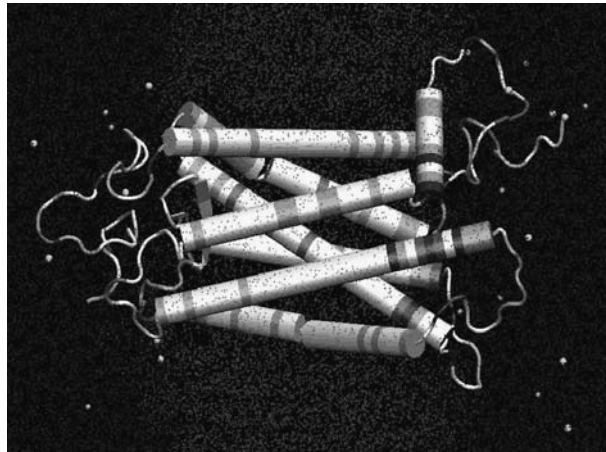
5.2 Topology change

The second test case was chosen to simulate changes in topology of a system. The system is similar to the one in the previous test case, i.e., it is made up of four rigid bodies connected by revolute joints to form a serial chain topology. The system starts from rest and swings under the effect of gravity. At a randomly chosen instant during the temporal simulation, the last body in the system is instantaneously connected to the inertial frame by a revolute joint. This reduces the system instantaneously from a serial chain to a kinematically closed loop configuration. After the event, the system continues to swing under gravity albeit with the first and last body in the system connected to the inertial frame. The system description and starting conditions for this test case are identical to the first test case discussed above. At a randomly chosen instant of $t = 0.7$ s, the last body of the system is instantaneously anchored to the inertial frame by a revolute joint. The values of the generalized coordinates and speeds are plotted in Fig. 4.

5.3 Coarse-graining in molecular dynamics system

While the two examples presented above are traditional multibody dynamics systems, an application is presented in this subsection associated with the use of this algorithm for coarse-graining molecular dynamics systems. This test case is aimed at correctly modeling systems where a number of kinematic constraints are simultaneously and instantaneously imposed on an initially unconstrained system in 3 dimensional space. The system studied is the Rhodopsin protein which is a G-protein coupled receptor with a defined tertiary structure. A cartoon representation of the protein is shown in Fig. 5. It is a good example to study

Fig. 5 Representation of Rhodopsin protein



transduction and a large amount of experimental results are available about its structure and function. This protein's light driven photo-cycle plays an essential role in generating visual response. In prior studies [28], it has been found to demonstrate relative rigid body motion between residues.

The fully atomistic model of the Rhodopsin protein consists of more than 5000 atoms. Based on the findings of [28], it is desirable to coarse-grain the fully atomistic domain in two stages to a reduced order articulated multi-rigid body system. The first step is to coarse-grain the atomistic system into 26 uncoupled (discrete) rigid bodies that interact only through noninertial interatomic forces. From the dynamics perspective, this is a simple process of aggregation where the mass, mass moments of inertia, and velocity of center of mass and angular velocity of the discrete rigid bodies can be easily generated from the data for the atomistic system by taking the appropriate summations and moments. Although this is a coarse-grained model, this discrete rigid body model still includes some stiff interatomic forces which limit the integration time step. Consequently, the next step in coarse-graining is to move to an articulated multi-rigid body model where the stiff interatomic forces are replaced by imposing constraints.

During the transition, the relative translational motion of consecutive bodies is constrained by imposing kinematic joints between successive bodies. Each kinematic joint is modeled as a spherical joint which instantaneously constraints the relative translation while allowing for relative rotation between two consecutive bodies. This instantaneous change in the system degrees of freedom introduces impulsive loads at each joint resulting in discontinuous jumps in the remaining generalized speeds. The articulated multi-rigid body model of the system consists of a free floating chain where the first (or last) body in the chain moves relative to the inertial reference frame by 3 translational and 3 rotational degrees of freedom while each successive body moves relative to its parent body by only 3 rotational degrees of freedom. In the discrete rigid body system, the generalized coordinates and generalized speeds used to model the orientation, position, translational and angular velocities for individual bodies were associated with the absolute coordinates of the bodies. However, in the articulated system, the generalized coordinates are used to map the relative orientations and positions of the bodies while the generalized speeds are used to model the relative angular velocities between two consecutive bodies. Thus the system model transitions between two completely different sets of generalized coordinates and speeds.

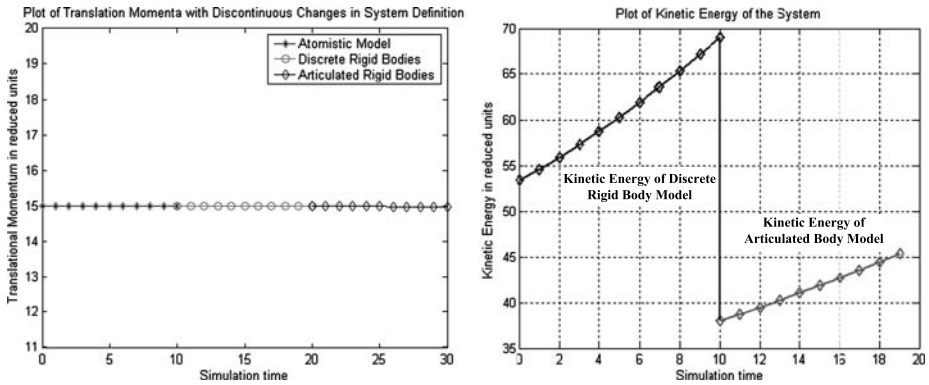


Fig. 6 Translational momentum and kinetic energy of different models

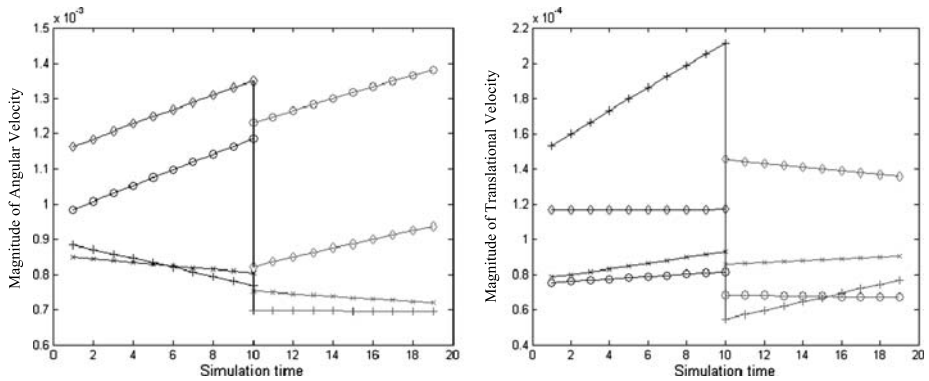


Fig. 7 Magnitudes of translational and angular velocities of representative bodies

The Fig. 6 shows the variations in the magnitude of translational momentum of the system as it transitions between the three models viz. fully atomistic, discrete rigid bodies and articulated rigid bodies. It also shows the kinetic energy of the system as it transitions from the discrete rigid body model to the articulated multi-rigid body model. The impulsive loads applied to coarse-grain the system are all internal to the system. Consequently, the momentum of the system is expected to be conserved and it is captured accordingly in the results of the simulations. The plots shows 10 integration steps with the three different models and the magnitude of the translational momentum remains conserved in these transitions. The components of the momentum along the different axes are also conserved but not shown here for clarity. As the system is being coarse-grained, a certain amount of kinetic energy of the system is expected to be lost. This aspect is demonstrated in the plot for kinetic energy where a step change in the energy is observed as the system transitions from the discrete to articulated models. Further, as the system is subjected to impulsive loads, the angular and translational velocities of the bodies is expected to undergo a step change. This behavior is also captured in the implementation of this algorithm and the Fig. 7 shows the variations in the magnitude of the translational velocity of the center of mass and the angular velocity of four representative bodies in the system.

5.4 Discussion

For the three systems simulated, the method was able to accurately simulate the instantaneous transitions in system description through a generalized impulse–momentum formulation in a divide and conquer scheme. The calculation of the jumps in the generalized speeds is computationally efficient, incurring $O(n)$ and theoretically $O(\log(n))$ cost in serial and parallel implementation. The first test case is a traditional problem which has been simulated previously [20] as a reduced model of a solar panel. The method is able to simulate this system correctly. The generalized speed associated with the locked joint goes to zero while there is a discontinuous jump in remaining generalized speeds. At the instant of the joint lock, there is no change in the generalized coordinates. However, following the event, the discontinuous jump in the generalized speeds is propagated through temporal integration and its effect is observed in the generalized coordinates as well. As expected, there is no change in the value of the generalized coordinate and the generalized speed associated with the locked joint during the remainder of the simulation. The remaining generalized coordinates and speeds continue to change in a continuous manner as the altered system moves under gravity.

The results of the second test case affirm the ability of the formulation to simulate an instantaneous change in system definition from serial chain to a closed loop topology. The instantaneous anchoring of the final body results in an impulsive load on the body from the inertial frame which instantaneously constrains out the translational motion of the last body relative to the inertial frame. This impulsive load is propagated through the system as constraint impulsive loads at the joints and results in discontinuous jumps in the values of the remaining generalized speeds. At the instant of anchoring, there is again no change in the generalized coordinates but the effects of temporal integration of the discontinuous change in generalized speeds are observed in the system behavior after the event.

The third system studied is an application of model resolution change where a molecular dynamics system is transitioned through models with three different resolutions. This model resolution change includes impulsive events at each joint of the 25 joints between the bodies in the system. In this study, only a small representative simulation was carried with only a total of 30 integration steps and only a single transition from a discrete to an articulated model. An actual simulation of significance involves approximately 10^9 integration steps and includes many different model resolution changes. The results presented here are for demonstrating the validity of the algorithm.

For the systems simulated, the generalized momenta of the system is expected to be conserved. All the impulsive loads acting on the system are constraint loads which are contained in the space orthogonal to the space of admissible motion of the system as spanned by the partial velocities (or joint free-motion maps) of the system after an event [29]. Hence, the projection of the momentum of the system before and after the event into the space of admissible motion after the event must be equal. Further, as certain degrees of freedom at specific kinematic joints are being instantaneously constrained, the kinetic energy associated with these degrees of freedom is lost and manifests in a discontinuous change in the system kinetic energy. This is an inherent feature of the physical behavior of such systems and is captured in the methodology through the properties of projection into the space of admissible motion.

The validity of the simulations is observed by plotting the generalized momenta of the system during the simulation. The results obtained from the implementation of the test cases clearly capture the conservation of the generalized momenta of the system during an event. In all cases, the generalized momenta associated with the unaffected generalized speeds

vary in a continuous manner and remain conserved during the event. In the results of the molecular dynamics system, only the translational momentum of the system is shown.

An important question that arises from using this algorithm is related to identifying where and when the model transition is warranted. A likely answer to this would be the usage of event prediction schemes which typically work in tandem with the temporal integration schemes. These are widely used for modeling impact between many bodies, for example, in granular material modeling. Indeed, for the systems similar to the first two systems studied in this work, an event prediction scheme would be required when the algorithm is applied for generalized usage. However, for molecular dynamics systems, the application of this algorithm is not for impact modeling and hence the traditional event prediction schemes are not appropriate. In such cases, two possible methods may be used to identify where and when to introduce the model transitions. The first is based on analysts' experience with the systems, where the large volume of experimental data on these systems and their structural information may be used to identify when and where to introduce the model transitions. The second approach is based on using concurrent analysis tools and adaptive metrics such as error indicators which monitor the system behavior based on its current and past states during the course of a temporal simulation and provide important information on where and when to apply the model transitions. Such schemes have been developed in other areas of computational mechanics such as in finite element methods [30] and are a major focus of research for molecular dynamics systems. While the validity and efficacy of these methods are pertinent questions, they are not relevant to the scope of this current work. The method developed here is focussed on how to correctly coarse-grain the models by imposing kinematic constraints such that the resulting model is kinematically correct and conserves the essential dynamics.

While the motivation of this work has been to put forward a methodology for modeling discontinuous changes in system definition, the method developed here is also applicable to certain classes of contact–impact problems. The method developed here is based on the projection of the momenta equations before and after an *event* into the space of admissible motion after the event. Consequently, if the method is used to model contact–impact, this projection into the space of admissible motion and its orthogonal complement would play the role of the impact law. Further, the method could be extended to include an explicit contact law, for example, as indicated in (7), with the necessary addition of a contact model dependent impulse term $\int_{t^-}^{t^+} \mathcal{F}_a^k dt$. This application of the method for contact–impact problems is not further pursued here. Instead the methodology for accommodating changes in system definitions as found in model resolution changes has been explored.

5.5 Computational complexity and parallel aspects

In serial implementation, the hierarchic assembly and disassembly processes work recursively and solve the impulse–momentum problem in linear or $O(n)$ complexity where n is the number of degrees of freedom of the system. The computational cost is comparable with the forward dynamics problem as studied in [22, 23]. For parallel implementation, this algorithm is processor and time optimal, solving the impulse–momentum problem in $O(\log(n))$ complexity in the presence of n processors, where n now is the number of bodies in the system. In the presence of n processors, each body of the system is mapped onto a different processor where the impulse–momentum problem for that body is formulated. The mapping of the bodies onto the processors is developed in a binary tree representation as shown in Fig. 2. The hierarchic assembly disassembly process then works via two traversals of the binary tree. These traversals work in exactly the same fashion as discussed in [31] and are

achieved in $O(\log(n))$ complexity. This highly parallel aspect of the algorithm arises from the nature of the impulse–momentum equations for individual bodies or assemblies. As discussed previously, the equations are cast in the *two handle* form where the problem is posed in terms of the interactions of the body or an assembly with its boundaries by expressing the internal unknowns as functions of boundary unknowns. This allows the assembly disassembly process to proceed in an order independent, concurrent form, facilitating high parallel efficiency.

In the presence of a modest number of processors, the system is divided into assemblies equal to the number of processors available. Within each processor, the equations of the corresponding assembly can be formulated in linear complexity to express the problem in terms of the boundary unknowns of the assembly, similar to the serial implementation. The calculation of the boundary unknowns proceeds using the binary tree representation of the system, where the leaf nodes now correspond to the assemblies instead of the physical bodies. This is achieved in logarithmic complexity. On completing this, the boundary unknowns of every assembly in the system are known. Using these values, the impulse–momentum equations of the bodies in each assembly can be solved in linear complexity using the recursive process as in the serial implementation. This linear complexity process is carried out concurrently for all assemblies. The number of bodies in the different assemblies and the actual computational gains would depend on different parameters such as load balancing, multi-processor architecture, the method for inter-processor communications and costs, among other implementation dependent aspects.

6 Conclusions

A methodology is outlined in this paper which is able to accurately and efficiently simulate discontinuous changes in system definition for multibody dynamics systems. The method accommodates the discontinuous changes by reformulating joint definitions locally within the affected bodies, without having to reformulate the equations for the entire system. As demonstrated, the changes in system definitions are modelled through the use of joint free-motion maps and impulsive constraint loads. This is implemented in an efficient divide and conquer formulation to provide linear and logarithmic complexity for serial and parallel implementations respectively. The method can also accommodate systems in what would normally be considered singular configurations. Results from simulations of two test cases are shown which demonstrate the validity of the method for systems with unilateral constraints and systems with both unilateral and bilateral constraints. An application in molecular dynamics simulations for model resolution changes is also demonstrated.

Acknowledgements This work was funded by the NSF NIRT Grant Number 0303902. The authors would like to thank the funding agency for their support.

References

1. Piedboeuf, J., Gonthier, Y., McPhee, J., Lange, C.: A regularized contact model with asymmetric damping and dwell-time dependent friction. *Multibody Syst. Dyn.* **11**, 209–233 (2004)
2. Bei, Y., Fregly, B.J.: Multibody dynamic simulation of knee contact mechanics. *Med. Eng. Phys.* **26**(9), 777–789 (2004)
3. Glocker, C., Pfeiffer, P.: Multiple impacts with friction in multibody systems. *Nonlinear Dyn.* **7**, 471–497 (1995)

4. Pfeiffer, F.G.: Applications of unilateral multibody dynamics. *Philos. Trans. Roy. Soc. Lond.* **359**(1789), 2609–2628 (2001)
5. Pfeiffer, F., Glocker, C.: *Multibody Dynamics with Unilateral Constraints*. CISM Courses and Lectures, vol. 421, International Centre for Mechanical Sciences. Springer, New York (2000)
6. Stewart, D.E.: Rigid-body dynamics with friction and impact. *SIAM Rev.* **42**(1), 3–39 (2000)
7. Ambrósio, J.A.C., Pereira, M.S., Dias, J.P.: Crashworthiness analysis and design using rigid-flexible multibody dynamics with applications to train vehicles. *Int. J. Num. Method. Eng.* **40**(4), 655–687 (1997)
8. Ambrósio, J.A.C., Pereira, M.S., Dias, J.P.: Contact and impact models for vehicle crashworthiness simulation. *Int. J. Crashworth.* **8**, 73–86 (2003)
9. Barhorst, D.: Issues in computing contact forces for non-penetrating rigid bodies. *Algorithmica* **10**, 292–352 (1993)
10. Keller, J.B.: Impact with friction. *J. Appl. Mech.* **53**(1), 1–4 (1986)
11. Lötstedt, P.: Mechanical systems of rigid bodies subject to unilateral constraints. *SIAM J. Appl. Math.* **42**(2), 281–296 (1982)
12. Trinkle, J., Zeng, D., Sudarsky, S., Lo, G.: On dynamic multi-rigid-body contact problems with Coulomb friction. *Z. Angew. Math. Mech.* **77**(4), 267–279 (1997)
13. Wu, S., Haug, E.J., Yang, S.M.: Dynamics of mechanical systems with Coulomb friction, stiction, impact and constraint addition–deletion. *Mech. Mach. Theory* **21**(5), 401–425 (1986)
14. Ferris, M.C., Mangasarian, O.L., Pang, J.S.: Complementarity: applications, algorithms and extensions. In: *Applied Optimization*, vol. 50. Kluwer Academic, Dordrecht (2001)
15. Brenan, K.E., Campbell, S.L., Petzold, L.R.: *Numerical Solutions of Initial-value Problems in Differential-Algebraic Equations*. North-Holland, New York (1989)
16. Anderson, K.S.: An order- n formulation for the motion simulation of general multi-rigid-body tree systems. *Comput. Struct.* **46**(3), 547–559 (1993)
17. Rosenthal, D.E.: An order n formulation for robotic systems. *J. Astronaut. Sci.* **38**(4), 511–529 (1990)
18. Jain, A.: Unified formulation of dynamics for serial rigid multibody systems. *J. Guid. Control Dyn.* **14**(3), 531–542 (1991)
19. Featherstone, R.: The calculation of robotic dynamics using articulated body inertias. *Int. J. Robot. Res.* **2**(1), 13–30 (1983)
20. Anderson, K.S., Sadowski, M.J.: An efficient method for contact/impact problems in multibody systems: tree topologies. In: *Proceedings of the Fourth International Symposium on Multibody Dynamics and Vibrations*, ASME Design Engineering Technical Conference 2003, (DETC03), number DETC03/VIB-48338, Chicago, IL, 2–6 September 2003
21. Seabra Pereira, M., Nikravesh, P.: Impact dynamics of multibody systems with frictional contact using joint coordinates and canonical equations of motion. *Nonlinear Dyn.* **9**, 53–71 (1996)
22. Featherstone, R.: A divide-and-conquer articulated body algorithm for parallel $O(\log(n))$ calculation of rigid body dynamics. Part 1: Basic algorithm. *Int. J. Robot. Res.* **18**(9), 867–875 (1999)
23. Mukherjee, R., Anderson, K.S.: An orthogonal complement based divide-and-conquer algorithm for constrained multibody systems. *Nonlinear Dyn.* **48**(1–2), 199–215 (2007)
24. Featherstone, R.: *Robot Dynamics Algorithms*. Kluwer Academic, New York (1987)
25. Mukherjee, R., Anderson, K.S.: A logarithmic complexity divide-and-conquer algorithm for multi-flexible articulated body dynamics. *J. Comput. Nonlinear Dyn.* **2**(1), 10–21 (2007)
26. Kim, S.S., Vanderploeg, M.J.: Generalized and efficient method for dynamic analysis of mechanical systems using velocity transforms. *J. Mech. Transm. Autom. Des.* **108**(2), 176–182 (1986)
27. Nikravesh, P.E.: Systematic reduction of multibody equations to a minimal set. *Int. J. Nonlinear Mech.* **25**(2–3), 143–151 (1990)
28. Forrest, L.R., Crozier, P.S., Stevens, M.J., Woolf, T.B.: Molecular dynamics simulation of dark-adapted rhodopsin in an explicit membrane bilayer: coupling between local retinal and larger scale conformational changes. *J. Mol. Biol.* **333**, 493–514 (2003)
29. Kane, T.R., Levinson, D.A.: *Dynamics: Theory and Application*. McGraw-Hill, New York (1985)
30. Flaherty, J.E., Loy, R.M., Ozturan, C., Shephard, M.S., Szymanski, B.K., Teresco, J.D., Ziantz, L.H.: Parallel structures and dynamic load balancing for adaptive finite element computations. *Appl. Numer. Math.* **26**(1–2), 241–263 (1998)
31. Featherstone, R.: A divide-and-conquer articulated body algorithm for parallel $O(\log(n))$ calculation of rigid body dynamics. Part 2: Trees, loops, and accuracy. *Int. J. Robot. Res.* **18**(9), 876–892 (1999)